3D Finite-Difference Method Using Discontinuous Grids

Shin Aoi and Hiroyuki Fujiwara

Abstract We have formulated a 3D finite-difference method (FDM) using discontinuous grids, which is a kind of multigrid method. As long as uniform grids are used, the grid size is determined by the shortest wavelength to be calculated, and this constitutes a significant constraint on the introduction of low velocity layers. We use staggered grids which consist of, on the one hand, grids with fine spacing near the surface where the wave velocity is low, and, on the other hand, grids whose spacing is three times coarser in the deeper region. In each region, we calculated the wavefield using velocity-stress formulation of second order accuracy and connected these two regions using linear interpolations. The second order finite-difference (FD) approximation was used for updating. Since we did not use interpolations for updating, the time increments were the same in both regions. The use of discontinuous grids adapted to the velocity structure resulted in a significant reduction of computational requirements, which is model dependent but typically one fifth to one tenth, without a marked loss of accuracy.

Introduction

As a method of seismic wave simulation, the finite-difference (FD) approximation has frequently been used to solve equations of motion numerically for a couple of decades (e.g. Boore, 1972; Kelly et al., 1976), and the formulation using staggered grids is commonly employed at present (e.g. Virieux, 1984, 1986; Levander, 1988; Graves, 1996). Many researches have been carried out, such as the research of free boundary conditions on the surface (e.g. Vidale and Clayton, 1986; Stacey, 1994; Pitarka and Irikura, 1996; Ohminato and Chouet, 1997), elastic and liquid medium boundary conditions as boundary conditions on the seabed (e.g. Okamoto, 1996), non-reflecting (e.g. Cerjan et al., 1985) and absorbing (e.g. Clayton and Engquist, 1977; Stacey, 1988; Higdon, 1991) boundary conditions to avoid the reflected waves from the boundary of a finite computational region, as well as the introduction of a double couple point source (e.g. Alterman and Karal, 1968; Vidale and Helmberger, 1987; Helmberger and Vidale, 1988; Frankel, 1993; Graves, 1996), which is a particular issue for applying finite-difference method (FDM) in seismology. The FDM is one of the most practical waveform simulation methods in use today.

The improvement in computer capacities has made it possible to carry out simulations of a three dimensional wavefield with realistic velocity models on a large scale, such as the ones for the Kanto Plane (e.g. Sato et al., 1998; Sugawara et al., 1997) and the Los Angeles Basin (e.g. Yomogida and Etgen, 1993; Olsen and Archuleta, 1996; Graves, 1998). However, despite its considerable influence on waveforms, the low velocity layer near the surface cannot be incorporated into such models. For example, in the Kobe area where extensive damage occurred in the 1995 Hyogoken-Nanbu Earthquake, numerous geophysical explorations such as a reflection survey, refraction survey, and microtremor observation were performed, and detailed 3D seismic wave velocity structures have been proposed (e.g. Huzita,

1996). Ground motion simulations performed by Iwata et al. (1998) and Pitarka et al. (1998) using a 3D FDM and models of the underground structure in the Kobe region successfully reproduced an extension of the severely damaged band of the earthquake. Meanwhile, due to the high values of the adopted shear wave velocity of the near-surface sediments, the amplitude of the simulated strong motions were smaller than those observed.

As long as uniform grids are employed, their size is determined by the shortest wavelength to be calculated. Thus, the entire region must be divided into small grids even when the layer of low velocity only occupies a small part. This considerably increases the computational requirements in terms of time and memory. Using the 3D FDM, in order to calculate up to the frequency N times higher, or in order to introduce low velocity layers in which the wave velocity is N times smaller (i.e. reduce the grid size to 1/N), N^3 more memory, and N^4 more computation time are required. Therefore, we cannot depend on the progress of computing capacities exclusively for computations on a large scale. Moreover, in order to perform the underground structure inversion (e.g. Aoi et al., 1995, 1997), it is necessary to calculate the waveforms many times, so a method enabling quick calculations of waveforms is required.

When the wavefield is calculated by the FDM, the grid size near the surface should be as small as possible for the following reasons:

- the wave velocity of the near-surface sediment is relatively low;
- the underground structure is extremely heterogeneous;
- free surface boundary conditions that must be imposed on the free surface tend to be unstable, and in many cases we are interested in waveforms at the surface;
- when the grid is staggered the wave-field variables are not defined at the same position;
- the energy of the surface waves is concentrated near the surface, and its group velocity is slower than S-wave velocity.

Pitarka et al. (1996) represents an attempt to evaluate the influence of the surface layer on the wavefield without dividing the region into small grids unnecessarily. In this method, the waveforms are first calculated by a 2D FDM using the structure model without the surface layer of low velocity. Then the effects of this layer on the waveforms are considered using the convolution of 1D transfer functions, evaluated by the propagator-matrix technique (Haskell, 1953). However, this method merely evaluates the influence of the shallow layer in an approximate way. Another approach is to take a coarser grid spacing by enhancing the accuracy of FD approximation, using such methods as an FDM with spatial difference of a higher order (e.g. Yomogida and Etgen, 1993) or a pseudospectral method (e.g. Furumura, 1992). However, the coarse grid spacing does not enable the modeling of detailed parts of the structure, and the computation accuracy is not sufficient in structures having discontinuities with a high contrast. In order to achieve a high level of accuracy in computation, it is necessary to use sufficiently small grids. Thus, if we wish to calculate waveforms by the FDM using models that include near-surface layers with low velocity, we need to employ non-uniform grids that are adapted to the velocity structure. There are two types of non-uniform grids, continuous and discontinuous.

Continuous grids are the grids with the optimal distribution of grid spacing achieved by continuous mapping. Examples of methods using continuous grids include refining the grid spacing in the vicinity of the free surface (e.g. Moczo, 1989; Carcione, 1992), reducing the grid spacing in the vicinity of the fault plane (e.g. Mikumo et al., 1987; Mikumo and Miyatake, 1993), refining the grid spacing within a given region (e.g. Pitarka, 1999) and making grids that generally follow the interfaces of media (e.g. Fornberg, 1988; Nielsen et al., 1994). These methods are free of artificial computational errors resulting from sudden changes in the grid spacing, since they allow for a continuous reduction in grid spacing. On the other hand, their shortcoming is that the number of grid points can be changed only along the coordinate axis.

With regard to discontinuous grids, the grid system consists of several regions, each of them having a uniform grid. This is a kind of

multigrid technique which is already in use in the field of fluid mechanics (e.g. McBryan et al, 1991). At the boundary of each region, the FDM has to be formulated in a way that maintains the continuity of the wavefield. Examples of waveform simulations by the FDM using discontinuous grids include reducing the grid spacing in the vicinity of the free surface (e.g. Moczo et al., 1996), refining the grid spacing in the vicinity of the borehole (e.g. Falk et al., 1996; Kessler and Kosloff, 1991) and avoiding grid spacing which is too small in the central part of the cylindrical coordinate (e.g. Furumura et al., 1998). However, these are all examples of 2D problems. Examples of hybrid methods using both grid systems include Jastram and Tessmer (1994).

Numerous issues of seismology deal with structures in which the wave velocity is lower in the shallower part and higher in the deeper part. In such cases, grids that are discontinuous in the vertical direction are often advantageous. This is due to the fact that as long as continuous grids are used, even in the deep part where the velocity is much higher, the number of grids in the horizontal direction cannot be reduced, and that accordingly, the grid spacing in the horizontal direction cannot become coarser. In the present paper, we present an FD technique that is based on a discontinuous grid. We also analyze its accuracy by comparisons with waveforms produced by the discrete-wavenumber method (DWNM) (Bouchon, 1981; Schmidt and Tango, 1986) and by the FDM using uniform grids.

Method

Formulation of the FDM with Discontinuous Grids

We used a discontinuous grid that consists of two regions with different grid spacing. Figure 1 shows the unit cell of the grid and the 3D discontinuous grid together with its cross-sections. The grid spacing of Region I is small (the grid spacings in directions x, y and z are Δx, Δy and Δz, respectively), whereas the grid spacing of Region II is three times

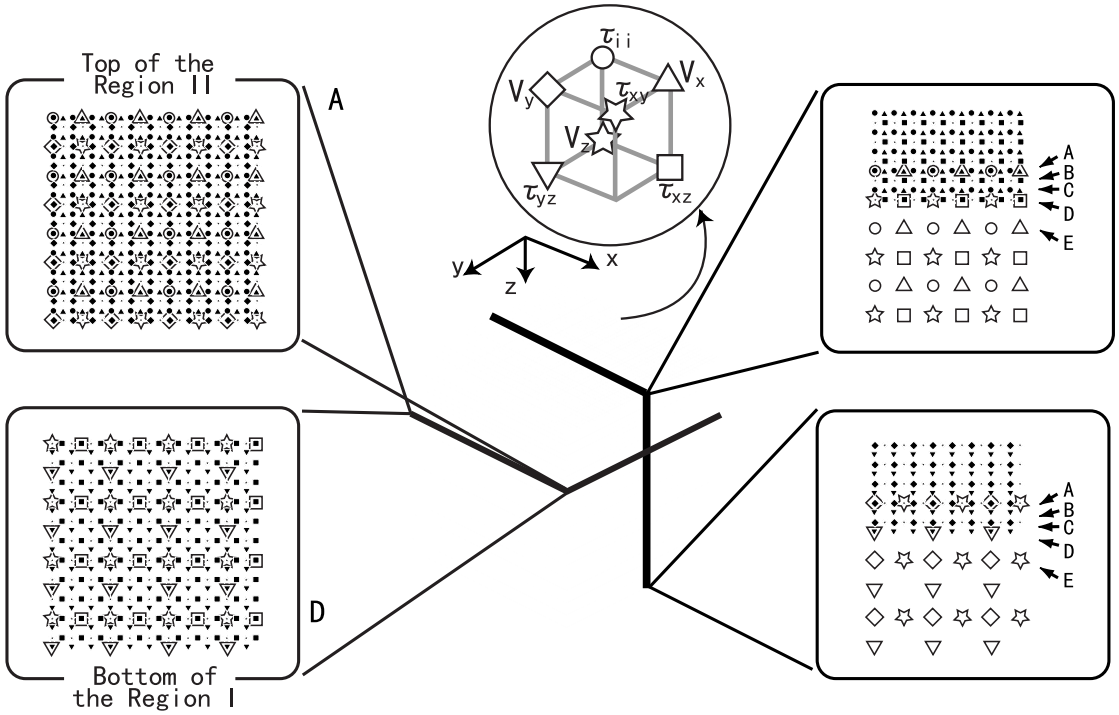

Fig. 1: (center) 3D discontinuous grid system and a unit cell for staggered grids (inside the circle). (left) Two transections on the top and at the bottom of the overlapping region of Regions I and II, where the elimination or the insertion of grid points are necessary. (right) Two profiles of the discontinuous grid. The arrows A-E show the overlapping region of Regions I and II, and the details of the interpolation are given in Table 1.

coarser (the grid spacings in directions x, y and z are $3\Delta x$, $3\Delta y$ and $3\Delta z$, respectively). In each region, a 3D staggered grid FDM of second-order accuracy in time and space is employed.

The discretized equations of motion are given by

$$
\begin{aligned}
v_{xi+1/2,j,k}^{n+1/2} &= v_{xi+1/2,j,k}^{n-1/2} \\
&+ \Delta t \times b\left[\frac{\tau_{xxi+1,j,k}^{n}-\tau_{xxi,j,k}^{n}}{\Delta x}+\frac{\tau_{xyi,j+1,k}^{n}-\tau_{xyi,j,k}^{n}}{\Delta y}\right. \\
&\left.+\frac{\tau_{xzi,j,k+1}^{n}-\tau_{xzi,j,k}^{n}}{\Delta z}\right] \\
v_{yi,j+1/2,k}^{n+1/2} &= v_{yi,j+1/2,k}^{n-1/2} \\
&+ \Delta t \times b\left[\frac{\tau_{xyi+1,j,k}^{n}-\tau_{xyi,j,k}^{n}}{\Delta x}+\frac{\tau_{yyi,j+1,k}^{n}-\tau_{yyi,j,k}^{n}}{\Delta y}\right. \\
&\left.+\frac{\tau_{yzi,j,k+1}^{n}-\tau_{yzi,j,k}^{n}}{\Delta z}\right] \\
v_{zi,j,k+1/2}^{n+1/2} &= v_{zi,j,k+1/2}^{n-1/2} \\
&+ \Delta t \times b\left[\frac{\tau_{xzi+1,j,k}^{n}-\tau_{xzi,j,k}^{n}}{\Delta x}+\frac{\tau_{yzi,j+1,k}^{n}-\tau_{yzi,j,k}^{n}}{\Delta y}\right. \\
&\left.+\frac{\tau_{zzi,j,k+1}^{n}-\tau_{zzi,j,k}^{n}}{\Delta z}\right]
\end{aligned}
\tag{1}
$$

and the discretized stress-strain relations are represented as

$$
\begin{aligned}
\tau_{xxi,j,k}^{n+1} &= \tau_{xxi,j,k}^{n} + \Delta t \times \left[(\lambda+2\mu)\frac{v_{xi+1/2,j,k}^{n+1/2}-v_{xi-1/2,j,k}^{n+1/2}}{\Delta x}\right. \\
&\left.+\lambda\left(\frac{v_{yi,j+1/2,k}^{n+1/2}-v_{yi,j-1/2,k}^{n+1/2}}{\Delta y}+\frac{v_{zi,j,k+1/2}^{n+1/2}-v_{zi,j,k-1/2}^{n+1/2}}{\Delta z}\right)\right] \\
\tau_{yyi,j,k}^{n+1} &= \tau_{yyi,j,k}^{n} + \Delta t \times \left[(\lambda+2\mu)\frac{v_{yi,j+1/2,k}^{n+1/2}-v_{yi,j-1/2,k}^{n+1/2}}{\Delta y}\right. \\
&\left.+\lambda\left(\frac{v_{xi+1/2,j,k}^{n+1/2}-v_{xi-1/2,j,k}^{n+1/2}}{\Delta x}+\frac{v_{zi,j,k+1/2}^{n+1/2}-v_{zi,j,k-1/2}^{n+1/2}}{\Delta z}\right)\right] \\
\tau_{zzi,j,k}^{n+1} &= \tau_{zzi,j,k}^{n} + \Delta t \times \left[(\lambda+2\mu)\frac{v_{zi,j,k+1/2}^{n+1/2}-v_{zi,j,k-1/2}^{n+1/2}}{\Delta z}\right. \\
&\left.+\lambda\left(\frac{v_{xi+1/2,j,k}^{n+1/2}-v_{xi-1/2,j,k}^{n+1/2}}{\Delta x}+\frac{v_{yi,j+1/2,k}^{n+1/2}-v_{yi,j-1/2,k}^{n+1/2}}{\Delta y}\right)\right] \\
\tau_{xyi+1/2,j+1/2,k}^{n+1} &= \tau_{xyi+1/2,j+1/2,k}^{n} + \Delta t \times \mu \\
&\left[\frac{v_{xi+1/2,j+1,k}^{n+1/2}-v_{xi+1/2,j,k}^{n+1/2}}{\Delta y}+\frac{v_{yi+1,j+1/2,k}^{n+1/2}-v_{yi,j+1/2,k}^{n+1/2}}{\Delta x}\right] \\
\tau_{xzi+1/2,j,k+1/2}^{n+1} &= \tau_{xzi+1/2,j,k+1/2}^{n} + \Delta t \times \mu \\
&\left[\frac{v_{xi+1/2,j,k+1}^{n+1/2}-v_{xi+1/2,j,k}^{n+1/2}}{\Delta z}+\frac{v_{zi+1,j,k+1/2}^{n+1/2}-v_{zi,j,k+1/2}^{n+1/2}}{\Delta x}\right] \\
\tau_{yzi,j+1/2,k+1/2}^{n+1} &= \tau_{yzi,j+1/2,k+1/2}^{n} + \Delta t \times \mu \\
&\left[\frac{v_{yi,j+1/2,k+1}^{n+1/2}-v_{yi,j+1/2,k}^{n+1/2}}{\Delta z}+\frac{v_{zi,j+1,k+1/2}^{n+1/2}-v_{zi,j,k+1/2}^{n+1/2}}{\Delta y}\right]
\end{aligned}
\tag{2}
$$

v_x, v_y, v_z represent the particle velocity, $t_{xx}, t_{yy}, t_{zz}, t_{xy}, t_{xz}, t_{yz}$ are the stress components, and f_x, f_y, f_z are the body force components. Δx, Δy and Δz represent the grid spacing in the x, y and z directions, respectively. Δt denotes the time increment. b is the buoyancy (inverse of density), and λ and μ are Lame constants. We used effective media parameters which were calculated using Grave's formulation (Graves, 1996). An elastic attenuation is introduced in the same way as in Graves (1996).

Only the field variables (velocity and stress components) that are adjacent to the variable to be updated are required to update the wavefield from the time level t_n to t_{n+1}. As it is clear from equations (1) and (2), when the FD approximation of second-order accuracy is employed for the spatial derivatives, the field variables that are within the distance of half-grid spacing in the x, y and z directions are required. Accordingly, only the field variables at the bottom plane of Region I and the top plane of Region II cannot be calculated by staggered grid FD operators (Fig. 1 and Table 1). Therefore, the field variables of these two planes must be calculated by inserting or eliminating the grids of the other region and by using interpolation of the wavefield across the two regions.

Table 1
How to up-date the time step of variables on each plane

	Region I	Region II
Region I	FDM	----
A	FDM	Interpolation
B and C	FDM	----
D	Interpolation	FDM
E	----	FDM
Region II	----	FDM

Table 2. Weights for linear interpolation.

l / x_i	0	1	2	3
	0	1/3	2/3	1
$a_i^0 = 1 - x_i$	1	2/3	1/3	0
$a_i^1 = x_i$	0	1/3	2/3	1

Interpolation

In this section we explain the technique used to interpolate the wavefield at the boundary between Regions I and II.

Regions I and II overlap in the vertical direction, covering the distance of $3\Delta z/2$. The field variables at the top plane of Region II cannot be obtained through the FD solutions. However, since the locations of the grid points at the top plane of Region II are identical to those of Region I, the field variables of the latter can be employed as those of the former (Fig. 1).

The field variables at the bottom of Region I are obtained by an interpolation scheme, using the field variables in Region II obtained by the FDM. What is interesting here is that the interpolations of all field variables are carried out within one horizontal plane, and that apart from these interpolations, the time updates of variables are carried out by the FD calculations (Table 1).

The linear functions

$$\begin{aligned} a^0(x) &= 1-x \\ a^1(x) &= x \end{aligned} \qquad (0 \le x \le 1) \tag{3}$$

are used for the interpolation. Table 2 indicates the weights for the interpolation obtained from these functions (equation (3)). These weights correspond to the points, x=0, 1/3, 2/3 and 1, when the grid reduction factor is 3.

The variables must be interpolated on the x-y plane at the bottom of Region I (Fig. 1, bottom left), and the grids are positioned as shown in Figure 2, where (I, J) and (i, j) are local indexings for the interpolation. The field variables obtained by the interpolation scheme are

$$u_{ij} = \sum_{I=0}^{1}\sum_{J=0}^{1} {}^{1}\alpha_{i,j}^{I,J} U^{I,J} \qquad (i,j = 0,1,2,3; I,J = 0,1) \tag{4}$$

$$\alpha_{i,j}^{I,J} = a_i^I \cdot a_j^J$$

where $U^{I,J}$ and $u_{i,j}$ indicate the field variables in Regions I and II, respectively.

Boundary Conditions

Boundary conditions are imposed to avoid artificial reflections from the boundary of the finite computational region. The most popular techniques used to avoid boundary reflections are absorbing (e.g. Clayton and Engquist, 1977; Stacey, 1988; Higdon, 1991), or non-reflecting (e.g. Cerjan et al., 1985) boundary conditions. The former is a method of realizing the boundary conditions that make the reflections of the body wave with a specific wavenumber vanish at a grid or a few grids in the vicinity of the boundary. The latter is a method of eliminating the reflected waves through their gradual attenuation by setting an absorbing region outside the boundary. Absorbing boundary conditions do have certain advantages in terms of computational requirements. However, apart from the case of the body wave with a specific wavenumber (normally a vertical incident wave), of which the reflections vanish, the method cannot realize a perfect absorption. On the contrary, approximately 10 to 20 % additional memory and computation are required to realize the non-reflecting boundary conditions. This method is capable of absorbing the waves almost completely regardless of whether it is a body wave (of any wavenumber) or a surface wave. Here we used the non-reflecting boundary conditions of Cerjan et al. (1985).

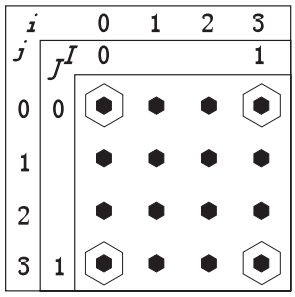

Fig. 2: Grid points location on the plane for interpolation, where (I, J) and (i, j) are local numberings for the interpolation.

In Cerjan et al. (1985), Gaussian functions given by

$$W = \exp(-\alpha(J_0 - j)^2), (j = 1,2,\cdots\cdots, J_0) \tag{5}$$

and

$$\begin{aligned} v_p^{n+1/2} &= W \cdot v_p^{n+1/2} \\ \tau_{pq}^n &= W \cdot \tau_{pq}^n \ (p,q = x,y,z) \end{aligned} \tag{6}$$

are used to attenuate the wavefield close to the boundary. According to Cerjan et al. (1985), $\alpha = 0.015$ and $J_0 = 20$ are the most appropriate values. Therefore these values are employed

in Region II. In Region I, $\alpha = 0.005$ and $J_0 = 60$ are employed because the process of attenuation must be continuous with Region II.

Though the number of grids $J_0 = 60$ in Region I is relatively large, the memory and computation time required to realize the non-reflecting boundary condition are negligible compared to those saved from the use of the discontinuous grids. Moreover, as the computation scale increases, the ratio of memory and computation used for the absorbing region to those used for the entire calculation decreases accordingly. For example, in a model with 2000*2000 grids in two horizontal directions, the ratio that the absorbing region occupies is less than 13 % of the entire region, and consequently, the increase of the computational requirement is hardly significant. However, in a case where the computational region is extremely flat, this ratio may become too significant to be neglected. One approach to solve this problem is to make the grid spacing in the absorbing region in Region I coarser, so that it will be identical to the grid spacing of Region II ($3\Delta x$, $3\Delta y$), thus reducing the number of grid points J_0 to 20. However, this approach is limited to structures in which the wave velocity is high near the absorbing boundary of Region I.

Stability Conditions

The stability condition for the constant grid spacing FD technique is

$$V_p \Delta t \sqrt{\frac{1}{\Delta x^2} + \frac{1}{\Delta y^2} + \frac{1}{\Delta z^2}} < 1 \qquad (7).$$

In the present method, this condition must be satisfied in both Regions I and II, because we use the constant grid spacing FD technique in each region. Since we do not use interpolations for updating the wavefield, the time increments are the same in both Regions I and II. This means that we use the minimum values of the time increments (Δt) determined by equation (7) for both regions.

Table 3
Physical parameters of the structure model

		Case 1	Case 2
Structure		Horizontally stratified structure	3-D basin structure
Shape		----------	Paraboloid of revolution Diameter 20 km Center x = -0.05 km, y = 0.0 km
Sediment	Vp	2.4 km/s	
	Vs	0.8 km/s	
	Density	1.8 km/s	
	Thickness/Max. depth	1.0 km	
Rock	Vp	4.3 km/s	
	Vs	2.5 km/s	
	Density	2.5 g/cm^3	

Table 4
Source parameters

	Case 1	Case 2
Source location	x=-1.2 km, y=-1.2 km, z= 9.4 km	
Source time function	Ricker wavelet (Tc = 3 sec)	
Source type	Single force point source (x-direction)	Double couple point source (strike=60°, rake=30°, dip=60°)

Examples of computation

The method proposed in this paper was used to calculate the waveforms in a 1D structure (horizontally stratified structure) and in a 3D basin structure. The results are compared with those obtained with a staggered grid FDM using uniform grids, in order to demonstrate the accuracy of the proposed method. The results obtained with the 1D structure are also compared to those of DWNM.

1D structure case

The structure is horizontally stratified and consists of two homogeneous layers the parameters of which are shown in Table 3. We use a single force point source acting in the x-direction which is located at (-1.2 km, -1.2 km, 9.4 km). Its source time function is a Ricker wavelet with a characteristic period of 3 sec. (Table 4).

Regarding the discontinuous grids employed in this calculation, their grid spacing is 100 m and 300 m in Regions I and II, respectively. The depths of Regions I and II are 1.5 km (15 grid points) and 18 km (60 grid points), respectively.

The time increments derived from the stability condition, equation (7), in Regions I and II are $\Delta t < 0.01343$ sec. and $\Delta t < 0.04049$ sec., respectively. Though the grid spacing in Region II is three times coarser than in Region I and the time increment can be three times longer accordingly, in our study the same time increment Δt = 0.0125 sec. is employed in both regions. The use of a longer time increment in Region II and the interpolations of time sampling can further reduce the computation time.

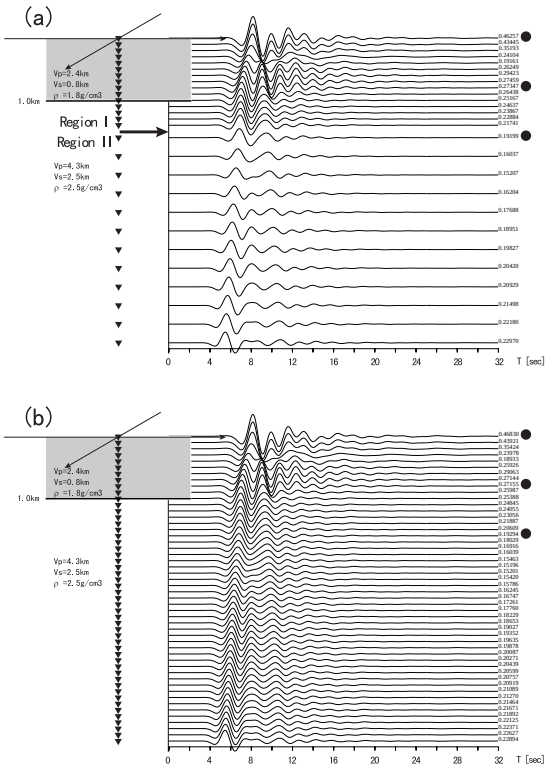

Fig. 3: Velocity waveform of the x-component at the observation points on the z-axis ($0\,km \le z \le 4.9km$, with spatial interval of 100 m. This interval is 300 m in Region II) in the 1D structure, calculated (a) by the FDM using discontinuous grids and (b) by the FDM using a uniform grid. The figures on the right are the maximum absolute value of amplitude (hereinafter maximum amplitude) of each waveform. On the left, the schematic of the structure employed is shown. The arrow indicates the boundary between the two regions.

Using a Ricker wavelet with a characteristic period of 3 sec. the minimum number of grids per wavelength in the entire computational region is 12.

In the computation using a continuous grid, the grid size is 100 m (155 grids in vertical direction) in the entire region of computation, and the time increment is identical to that of the computation with the discontinuous grid.

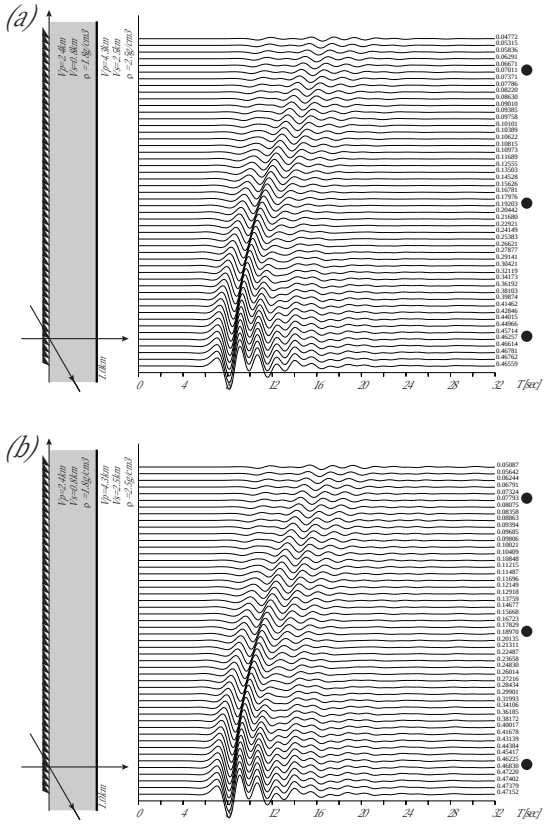

Fig. 4: Velocity waveforms of the x-component at the observation points on the x-axis ($-2.0km \le x \le 22.5km$, with an interval of 500 m) in the 1D structure, calculated (a) by the FDM using discontinuous grids and (b) by the FDM using uniform grids. The figures on the right are the maximum amplitude of each waveform. On the left, the schematic of the structure employed is shown.

Figure 3 compares synthetic seismograms calculated at a vertical receivers array with the proposed scheme using a discontinuous grid and the uniform grid scheme. The array covers the depth range between 0.0km and 4.9km and the interval between stations is 100m (300m interval for Regions II). There is an excellent match between the waveforms computed with the two grids. This indicates a high level of accuracy of the linear interpolation at the boundary between the two Regions. The accuracy is also confirmed by the continuous propagation of the wave passing the boundary (shown by the arrow) which is characterized by

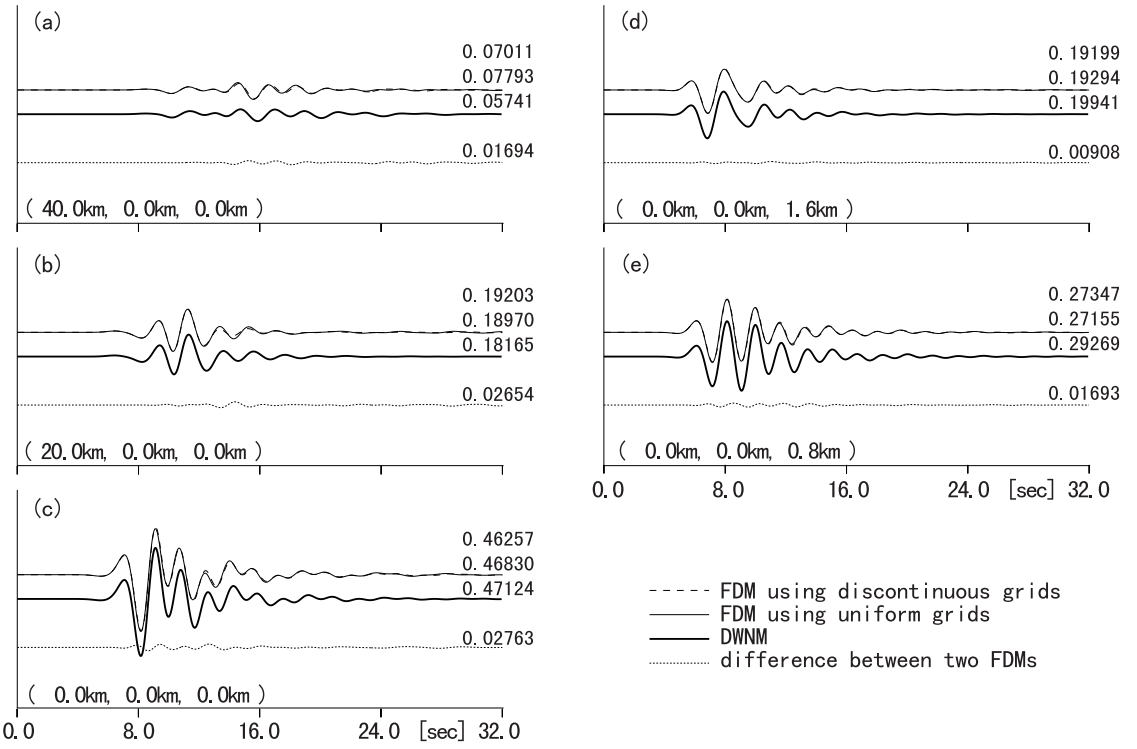

Fig. 5: The results of computation, by the FDM using discontinuous grids (dashed line), the FDM using uniform grid (thin line) and the DWNM (thick line). The waveforms in the lower part of the figure (dot line) show the difference in the results by the FDMs using the uniform grids and those using discontinuous grids. On the right of each waveform, the maximum and minimum amplitudes are indicated.

the absence of artificial reflected waves or disturbed waves (Fig. 3 (a)).

Figure 4 shows the comparison of synthetic seismograms calculated at receivers on the free surface. The receivers are aligned along the x-axis (-2.0km to 22.5km) and their spatial interval is 500m. As in the previous case, the comparison between the waveforms computed with the two techniques is very good.

In order to examine in detail the errors of the proposed scheme, the waveforms obtained by the FDM using a discontinuous grid, the FDM using uniform grids and the DWNM, at the observation points shown by circles in Figures 3 and 4, are shown in Figure 5. The bottom traces of each figure are the differences between the result from the FDM using a discontinuous grid and the one using uniform grid. As shown in Figure 5, all three methods resulted in amplitude and arrival times for all phases that are almost identical. At all receivers, the differences in amplitude is within 15 % of that calculated with the FDM using uniform grids except for the observation points which are far from the epicenter and whose amplitude is small. Moreover, the corresponding results of the FDM and the DWNM indicate a sufficiently high level of accuracy of the former one.

3D basin structure case

Here, synthetic seismograms calculated with the proposed FDM using discontinuous grid are compared to those of an FDM using uniform grid. In order to check the accuracy of the present method in the case of a more complex structure we used a basin model (Table 3). The basin model consists of a homogenous half space (bedrock) and a homogenous sedimentary layer. The basin geometry is a half paraboloid with a diameter of 20km and maximum depth of 1.0 km. The center of the paraboloid is at x=-0.05 km and y=0.0 km. The grids and source location employed for the computation are identical to those used in the 1D case. The source is a double couple point source with the strike, rake and dip angles of 60°, 30° and 60°, respectively (Table 4).

Figures 6 (a) and (b) show the comparison of the synthetic seismograms calculated with the FDM using both discontinuous grids and uniform grid at observation points having the same locations as in the 1D case.

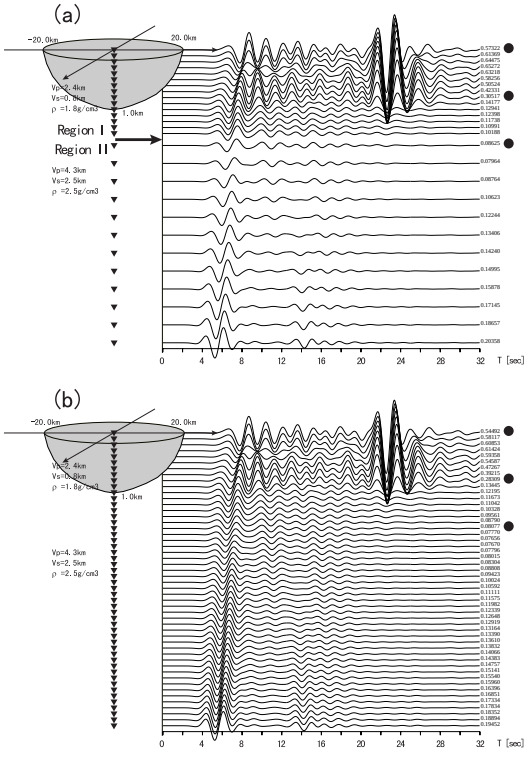

Fig. 6: Velocity waveform of the x-component at the observation points on the z-axis ($0\,km \le z \le 4.9km$, with an interval of 100 m. This interval is 300 m in Region II) in a 3D basin structure, calculated (a) by the FDM using discontinuous grid and (b) by the FDM using uniform grid. The figures on the right are the maximum amplitude of each waveform. On the left, the schematic of the structure employed is shown. The arrow indicates the boundary

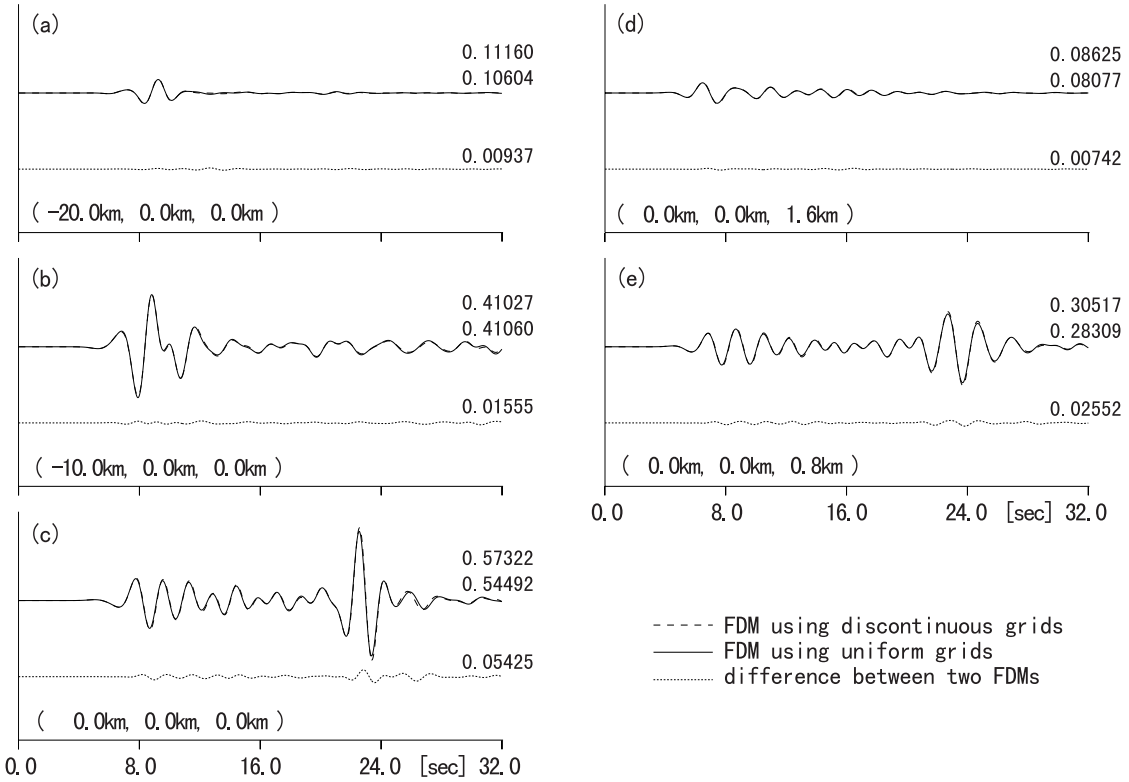

Fig. 7: The results of computation by the FDM using discontinuous grids (dashed line) and the FDM using uniform grid (thin line). The waveforms in the lower part of the figure (dot line) show the differences between them. The maximum amplitude is indicated on the right of each waveform.

The basin induced surface waves are dominant. In spite of the complicated wavefield, both methods resulted in amplitude and arrival times for all of the phases that are almost identical, as in the 1D case. The absence of reflected waves or disturbed waves at the artificial boundary between Regions I and II indicates that the wave is continuously propagated. The fact that surface waves are trapped by the sedimentary layer indicates the importance of high computational accuracy in the surface layer, which means the importance of using small grid spacing in the surface layer.

Figure 7 shows the waveforms of the x-component at five observation points. Waveforms show an excellent agreement and the differences between the result from the FDM with two kinds of grids are within 10 % at all of the observation points.

In both 1D and 3D model cases, the use of the discontinuous grid enables us to save computation time and memory to approximately 1/4.5 of what was needed when the uniform grid is used.

Discussions

In synthesizing waveforms by the FDM using discontinuous grids, the most important point is the accuracy of interpolations. In order to assist the quantitative evaluation of the accuracy of the linear interpolation scheme employed in this study, the interpolation of the 1D problem is considered here. One period of the cosine function,

$$f(x)=\begin{cases}(1+\cos 2\pi x/\lambda)/2 & (-\lambda/2\le x\le\lambda/2)\\ 0 & (x<-\lambda/2,\quad \lambda/2<x)\end{cases} \quad (9),$$

is discretized by the spatial interval ΔX, and each discretized point is called x_j. The cosine function discretized with 10 grid points per wavelength (i.e. $\lambda/\Delta X=10$) is shown in Figure 8 (a). This function is resampled, with an interval of Δx (which is $\Delta X/3$), using linear interpolations. The discretized points are denoted by x_i. Figure 8 (b) shows the resampled function, and Figure 8 (c) indicates the difference between the discretized function

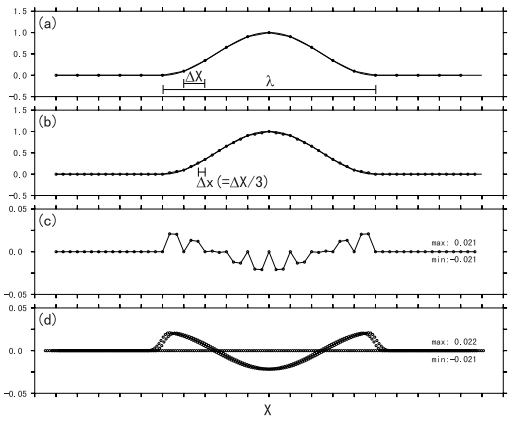

Fig. 8: Evaluation of error in the linear interpolation. (a) Cosine function discretized with 10 grid points per single wavelength (i.e. $\lambda/\Delta X = 10$). (b) Resampled function with ane interval of (which is $\Delta X/3$), using linear interpolations. (c) Difference between the discretized function and the exact value of the original function. (d) Evaluation of differences, repeated 10 times, shifting the sampling points X_j by $\Delta X/10$ each time. In this case, the error of interpolation is 0.022 (2.2 %).

and the exact value of the original function. The maximum absolute value of this difference divided by the maximum absolute value of the function, which is 1.0, is defined as the interpolation error:

$$error = \max\left| f_i - f(x_i) \right| / \max\left| f(x) \right| \qquad (10).$$

f_i shows the values of the discretized function at resampling points x_i. In this case, the interpolation error is 2.1 % (0.021). The values of interpolation error show some changes when the sampling points are shifted in the space. The evaluation of errors is repeated 10 times, shifting the sampling points X_j by $X_j/10$ each time. These interpolation errors are shown in Figure 8 (d), and as a result, in the case of $\lambda/\Delta X = 10$, the interpolation error of the interpolation is 2.2 %. The evaluation of the interpolation error is performed for a case where $\lambda/\Delta X$ is 3 to 15; the outcome is shown in Figure 9. According to this figure, the accuracy of the interpolation increases monotonously when the grid spacing becomes smaller. Based on the sampling criterion of the FD approximation of second-order accuracy, the grid spacing should satisfy the condition $\lambda/\Delta X > 10$ (e.g. Virieux, 1986), and accordingly, the accuracy of the interpolation is more than 2.2 %. As we explained earlier, the interpolation of each field variable is performed on a horizontal plane, which means that we apply a 2D interpolation. However, its accuracy is almost the same as that of the 1D interpolation, because the interpolations in the x- and y-directions are carried out independently. This analysis shows that a sufficient accuracy is obtained by using the linear interpolation, in an FD approximation of second-order accuracy is employed.

We have discussed the relation between the wavelength of the cosine function and the errors by linear interpolations. Although it is important to examine how the interpolation errors propagate through the wave equation which is sensitive to discretized partial derivatives, it is difficult to separate the errors due to the interpolation scheme alone from those caused by the grid dispersion and non-reflecting boundaries. Compared with such errors that are thought to be small enough in the applications, interpolation errors are of the same order or smaller. This means that the interpolation method we used has a sufficient level of accuracy. The problem of error propagation has to be solved in the future.

We also evaluated the ratio κ, which

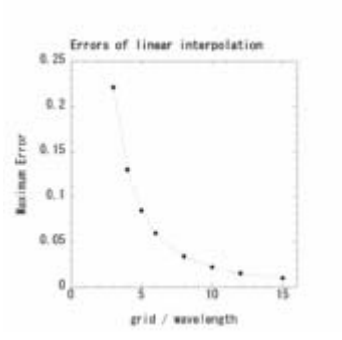

Fig. 9: Errors of linear interpolation. The errors of interpolation become smaller when the number of grid per single wavelength is smaller. When it is less than 10, the error of interpolation is less than 2.2 %.

represents the memory saving by the present method in comparison with the constant grid spacing FD technique. When $N \cdot \Delta x \times M \cdot \Delta y \times L \cdot \Delta z$ represents the entire region to be calculated, and the depth of Region I is given by $l \cdot \Delta z$,

$$\kappa = \frac{1/27\,(N + 6J_0)(M + 6J_0)(26l + L + 3J_0)}{(N + 2J_0)(M + 2J_0)(L + J_0)} \qquad (11).$$

If $M = N = L$ and $J_0 \ll N$ are assumed, then

$$\kappa = 1/27\left(1 + 26\frac{l}{L}\right) \times \left(1 + \frac{10J_0}{N}\right) \qquad (12).$$

$(1+26l/L)/27$ is a term representing how much memory is saved by using a grid which is three times coarser in Region II, and $1+10J_0/N$ is a term representing the disadvantage resulting from the larger absorbing region of Region I. The typical value of l/L being approximately 1/10 to 1/20, $(1+26l/L)/27$ is approximately 1/10. When N is 2000, $1+10J_0/N$ is 1.1, which is a loss that can be neglected. The computation time for interpolations is less than a few percent of the entire computation time. Thus, a ratio similar to the case of the memory is saved in computation time as well, that results in an approximately tenfold saving of both memory and time. This signifies that the introduction of the present method can reduce the grid spacing to less than half without imposing an additional load on the computers.

Conclusions

One of the biggest problems in 3D wave propagation modeling using the FDM with a uniform grid is the high computational requirements. These requirements are related to the oversampling of the models due to the constant grid spacing in the region with high velocity. In order to avoid oversamping it is necessary to use non-uniform grids that are adapted to the velocity structure. In this study we used a discontinuous grid that consists of two regions of different grid spacing. The grid spacing ratio between the two regions was a factor of three. By connecting these two regions by eliminating or inserting grids, we have succeeded in dramatically reducing the computational requirements, without significantly diminishing the accuracy of the calculation. In the case where Region I occupies 10 % of entire region, we can reduce the computational requirements to approximately 1/10 and this means that the grid spacing can be reduced to less than half without increasing the computational requirements.

The examination of the accuracy of linear interpolation employed in this study by a simple cosine function showed that the accuracy increases monotonously when the grid spacing ΔX decreases. It was also shown that when the number of grid points per wavelength is more than 10, the interpolation error is less than 2.2 %. Accordingly, as long as an FD approximation of second-order accuracy is employed, which means $\lambda / \Delta X$ must be more than 10, a sufficient level of accuracy is obtained by using the linear interpolation.

A more flexible grid system will be further realized by increasing the number of the regions, and/or by using the hybrid methods that combine discontinuous grids with variable spacing. Also the interpolation of the time sampling can reduce the number of time increments, rendering the computation time ever shorter.

Acknowledgments

Discussions with Peter Moczo and Ralph J. Archuleta provided valuable insights that improved the paper. The reviews by Jean Virieux and Arben Pitarka were helpful in improving the quality and clarity of the manuscript. Yuko Kase pointed out many of the references on FDM. Computation time was provided by the Supercomputer Center of the National Research Institute for Earth Science and Disaster Prevention.

References

Aoi, S., T. Iwata, K. Irikura and F. J. Sanchez-Sesma (1995). Waveform inversion for determining the boundary shape of a basin structure, *Bull. Seism. Soc. Am.* **85**, 1445-

1455.

Aoi, S., T. Iwata, H. Fujiwara, and K. Irikura, (1997). Boundary Shape Waveform inversion for Two-Dimensional Basin Structure Using Three-Component Array Data with Obliquely Azimuthal Plane Incident Wave, *Bull. Seism. Soc. Am.* **87**, 222-233

Alterman, Z. and F. C. Karal, Jr. (1968). Propagation of elastic waves in layered media by finite difference methods, *Bull. Seism. Soc. Am.* **58**, 367-398.

Boore, D. M. (1972). Finite difference methods for seismic wave propagation in heterogeneous materials, in *Methods in Computational Physics*, Vol.11, B. A. Bolt (Editor), Academic Press, New York.

Bouchon, M., (1981). A simple method to calculate Green's functions for elastic layered media, *Bull. Seism. Soc. Am.* **71**, 959-971.

Carcione, J. M. (1992), Modeling anelastic singular surface wave in the earth, *Geophysics* **57**, 781-792.

Cerjan, C., D. Kosloff, R. Kosloff, and M. Reshef (1985). A nonreflecting boundary condition for discrete acoustic and elastic wave equations, *Geophysics* **50**, 705-708.

Clayton, R. and B. Engquist (1977). Absorbing boundary conditions for acoustic and elastic wave equations, *Bull. Seism. Soc. Am.* **67**, 1529-1540.

Falk, J., E. Tessmer, and D. Gajewski (1996). Tube wave modeling by the finite-difference method with varying grid spacing, *PAGEOPH* **148**, 77-93.

Fornberg, B. (1988). The pseudospectral method: Accurate representation of interfaces in elastic wave calculations, *Geophysics* **53**, 625-637.

Frankel, A. (1993). Three-dimensional simulation of ground motion in the San Bernardino valley, California, for hypothetical earthquakes on the San Andreas fault, *Bull. Seism. Soc. Am*, **83**, 1020-1041

Furumura, T., (1992). Studies on the pseudospectral method for the synthetic seismograms, doctor thesis of Hokkaido Univ. (in Japanese).

Furumura, T., B. L. N. Kennett and M. Furumura (1998). Numerical modeling of seismic wave propagation in laterally heterogeneous whole Earth using the pseudospectral method, *abstracts of 1998 Japan Earth and Planetary Science Joint Meeting*, 282.

Graves, R. W. (1996). Simulating seismic wave propagation in 3D elastic media using staggered-grid finite differences, *Bull. Seism. Soc. Am.* **86**, 1091-1106.

Graves, R. W. (1998). Three-dimensional finite-difference modeling of the San Andreas fault: Source parameterization and ground-motion Levels, *Bull. Seism. Soc. Am.* **88**, 881-897.

Haskell, N. A. (1953). The dispersion of surface waves in multilayered media, *Bull. Seism. Soc. Am.* **43**, 17-34.

Helmberger, D. V. and J. E. Vidale (1988). Modeling strong motions produced by earthquakes with two-dimensional numerical codes, *Bull. Seism. Soc. Am.* **78**, 109-121.

Higdon, R. L. (1991). Absorbing boundary conditions for elastic waves, *Geophysics* **56**, 231-241.

Huzita, K. (1996). On survey results of active faults in Osaka-Kobe area, Proc. 9th seminar on studying active faults 'on deep structure of Osaka-bay area', 1-11, June (in Japanese).

Iwata, T., H. Sekiguchi, A. Pitarka, K. Kamae and K. Irikura (1998). Evaluation of strong ground motions in the source area during the 1995 Hyogoken-Nanbu (Kobe) earthquake, submitted to Proc. of the 10th Japan Earthquake Engineering Symposium.

Jastram, C. and E. Tessmer (1994). Elastic modelling on a grid with vertically varying spacing, *Geophysical Prospecting* **42**, 357-370.

Kelly, K. R., R. W. Ward, S. Treitel, and R. M. Alford (1976). Synthetic seismograms: a finite-difference approach, *Geophysics* **41**, 2-27.

Kessler, D. and D. Kosloff (1991). Elastic wave propagation using cylindrical coordinates, *Geophysics* **56**, 2080-2089.

Levander, A. R. (1988). Fourth-order finite-difference *P-SV* seismograms, *Geophysics* **53**, 1425-1436.

McBryan, O. A., P. O. Frederickson, J. Linden, A. Schuller, K. Solchenbach, K. Stuben, C. A. Thole and U. Trottenberg (1991), Multigrid methods on parallel computers ----- a survey of recent developments, *Impact comput. sci. engrg.* **3**, 1-75

Mikumo, T., K. Hirahara, and T. Miyatake (1987). Dynamical fault rupture processes in heterogeneous media, *Tectonophysics* **144**, 19-36.

Mikumo, T. and T. Miyatake (1993). Dynamic rupture processes on a dipping fault, and estimates of stress drop and strength excess from the results of waveform inversion, *Geophys. J. Int.* **112**, 481-496.

Moczo, P. (1989). Finite-difference technique for *SH*-waves in 2-D media using irregular grids – application to the seismic response problem, *Geophys. J. Int.* **99**, 321-329.

Moczo, P., P. Labák, J. Kristek, and F. Hron (1996). Amplification and differential motion due to an antiplane 2D resonance in the sediment valleys embedded in a layer over the half-space, *Bull. Seism. Soc. Am.* **86**, 1434-1446.

Nielsen, P., F. If, P. Berg, and O. Skovgaard (1994). Using the pseudospectral technique on curved grids for 2D acoustic forward modelling, *Geophysical Prospecting* **42**, 321-341.

Ohminato, T. and B. A. Chouet (1997). A free-surface boundary condition for including 3D topography in the finite-difference method, *Bull. Seism. Soc. Am.* **87**, 494-515.

Okamoto, T. (1996). Complete near-field 2.5D finite difference seismograms for shallow subduction zone earthquakes, *abstracts of 1996 Fall Meeting of the Seismological Society of Japan*, P09.

Olsen B. K., Ralph J. Archuleta (1996). Three-dimensional simulation of earthquakes on the Los Angeles fault system, *Bull. Seism. Soc. Am*, **86**, 575-596.

Pitarka, A. (1999). 3D elastic finite-difference modeling of seismic motion using staggered grids with nonuniform spacing, *Bull. Seism. Soc. Am.*, **89**, 54-68.

Pitarka, A. and K. Irikura (1996) Modeling 3D surface topography by finite-difference method: Kobe-JMA Station Site, Japan, case study, *Geophys. Res. Lett.* **23**, 2729-2732.

Pitarka, A., K. Irikura, T. Iwata, and T. Kagawa (1996). Basin structure effects in the Kobe area inferred from the modeling of ground motions from two aftershocks of the January 17, 1995, Hyogo-ken Nanbu Earthquake, *J. Phys. Earth*, **44**, 563-576.

Pitarka, A., K. Irikura, T. Iwata, and H. Sekiguchi (1998). Three-dimensional simulation of the near-fault ground motion for the 1995 Hyogo-ken Nanbu (Kobe), Japan, earthquake, *Bull. Seism. Soc. Am.*, **88**, 428-440

Sato, T., R. W. Graves, P.G. Somerville and S. Kataoka (1998). Estimates of regional and local strong motions during the Great 1923 Kanto, Japan, Earthquake (*Ms* 8.2). Part 2: Forward simulation of seismograms using variable-slip rupture models and estimation of near-fault long-period ground motions, *Bull. Seism. Soc. Am.* **88**, 206-227.

Schmidt, H. and G. Tango (1986). Efficient global matrix approach to the computation of synthetic seismograms, *Geophys. J. R. astr. Soc.*, **84**, 331-359.

Stacey, R. (1988). Improved transparent boundary formulations for the elastic-wave equation, B*ull. Seism. Soc. Am.* **78**, 2089-2097.

Stacey, R. (1994). New finite-difference methods for free surfaces with a stability analysis, *Bull. Seism. Soc. Am.* **84**, 171-184.

Sugawara, O., T. Yamanaka and M. Kamata (1997). Simulation of 3D-wave propagation in the Kanto Basin during the 1923 Kanto Earthquake, *abstracts of 1997 Japan Earth and Planetary Science Joint Meeting*, 108 (in Japanese).

Vidale, J. E. and Clayton R. W. (1986). A stable free-surface boundary condition for two-dimensional elastic finite-difference wave simulation, *Geophysics* **51**, 2247-2249.

Vidale, J. E. and D. V. Helmberger (1987). Path effects in strong motion seismology, in *Seismic Strong Motion Synthetics*, (Editor B. Bolt), Academic Press, New York.

Virieux, J. (1984). *SH*-wave propagation in heterogeneous media: Velocity-stress

finite-difference method, *Geophysics* **49**, 1933-1957.

Virieux, J. (1986). P-SV wave propagation in heterogeneous media: Velocity-stress finite-difference method, *Geophysics* **51**, 889-901.

Yomogida, K. and J.T. Etgen (1993). 3-D wave propagation in the Los Angeles Basin for the Whittier-Narrows Earthquake, *Bull. Seism. Soc. Am.* **83**, 1325-1344.

National Research Institute for Earth Science and Disaster Prevention
3-1 Tenoudai, Tsukuba-city, Ibaraki 305 Japan
aoi@geo.bosai.go.jp
(S. A., H. F.)